Quaternary Science Reviews 170 (2017) 45–55

Contents lists available at ScienceDirect

Quaternary Science Reviews

journal homepage: www.elsevier.com/locate/quascirev

Holocene temperatures and isotopes of precipitation in Northwest Greenland recorded in lacustrine organic materials

G. Everett Lasher [a, *], Yarrow Axford [a], Jamie M. McFarlin [a], Meredith A. Kelly [b], Erich C. Osterberg [b], Max B. Berkelhammer [c]

[a] Department of Earth and Planetary Sciences, Northwestern University, Evanston, IL 60208, USA
[b] Department of Geological Sciences, Dartmouth College, Hanover, NH 03755, USA
[c] Department of Earth and Environmental Sciences, University of Illinois at Chicago, Chicago, IL 60607, USA

ARTICLE INFO

Article history:
Received 17 November 2016
Received in revised form
14 June 2017
Accepted 15 June 2017

Keywords:
Holocene
Paleolimnology
Paleoclimatology
Greenland
Stable isotopes
Chironomids

ABSTRACT

Reconstructions of Holocene lake water isotopic composition based upon subfossil aquatic organic material offer new insights into Arctic climate. We present quantitative estimates of warmth during the Holocene Thermal Maximum in northwest Greenland, inferred from oxygen isotopes of chironomid head capsules and aquatic moss preserved in lake sediments. $\delta^{18}O$ values of chironomids from surface sediments of multiple Greenland lakes indicate that these subfossil remains record the $\delta^{18}O$ values of the lake water in which they grow. Our lake water $\delta^{18}O$ reconstruction is supported by downcore agreement with $\delta^{18}O$ values in aquatic moss and chironomid remains. $\delta^{18}O$ of both organic materials from Secret Lake decrease after 4 ka (ka = thousands of years ago) by 3‰ into the Neoglacial. We argue that lake water at Secret Lake primarily reflects precipitation $\delta^{18}O$ values, which is strongly correlated with air temperature in NW Greenland, and that this signal is biased towards summer and early autumn conditions. Other factors may have influenced Secret Lake $\delta^{18}O$ values through the Holocene, including evaporation of lake water and changing seasonality and source of precipitation. The maximum early Holocene summer and early autumn-biased temperature anomaly at Secret Lake is 2.5–4 °C warmer than present from 7.7 (the beginning of our record) to ~6 ka. The maximum late Holocene cold anomaly (which includes the Little Ice Age) is 1.5–3 °C colder than present. These ranges of possible temperature anomalies reflect uncertainty in the $\delta^{18}O$ – temperature relationship for precipitation at the study site through the Holocene.

1. Introduction

By the end of this century, temperatures are predicted to increase in the Arctic between 2 and 9 °C (Stocker et al., 2013). Reducing the uncertainty around these estimates has important societal implications, and studies of past climate conditions can help clarify how climate change may occur in the Arctic. During an early to middle Holocene Thermal Maximum (HTM), summers were warmer than present across most of the Arctic between 9 and 5 ka, driving the most extensive retreat of the Greenland ice sheet (GrIS) since the end of the last glacial maximum at ~11 ka (Lecavalier et al., 2014). This time period provides an opportunity to test the sensitivity of the GrIS to the most recent sustained warm period in the Arctic, however the magnitude and spatiotemporal expression of the HTM in Greenland (and the Arctic as a whole) was heterogeneous and is not yet fully characterized (Briner et al., 2016; Kaufman et al., 2016). Climate records in northwest Greenland are sparse, leaving the timing and magnitude of the HTM in this sector of the Arctic largely unresolved. Estimates of sea surface temperatures in nearby Baffin Bay (Levac et al., 2001) and air temperature estimates based upon oxygen isotopes ($\delta^{18}O$) in the Agassiz ice core (Lecavalier et al., 2013, 2017) and pollen in lake sediments (Gajewski, 2015) provide evidence for temperature shifts at nearby sites during the Holocene, but differ in the timing and magnitude of past warmth. Additional proxy records from beyond the Greenland Ice Sheet will aid in clarifying the region's climate response to solar insolation trends.

To reconstruct a Holocene climate history for the Thule region of northwest Greenland, we employ $\delta^{18}O$ values from analyses of subfossil aquatic organic material in lake sediments. We measured $\delta^{18}O$ of chironomid larval head capsules and aquatic moss stems

* Corresponding author.
E-mail address: everett@earth.northwestern.edu (G.E. Lasher).

http://dx.doi.org/10.1016/j.quascirev.2017.06.016
0277-3791/

preserved in the sediments of a precipitation-fed lake to infer past lake water isotopic composition and, by extension, interpret possible climatic controls on precipitation $\delta^{18}O$. Previous work has demonstrated that $\delta^{18}O$ values of chironomid head capsules reflects the isotopic composition of the water in which they grow in both laboratory culturing experiments and modern lakes (Mayr et al., 2015; Verbruggen et al., 2011; Wang et al., 2009; Wooller et al., 2004), and we report chironomid $\delta^{18}O$ values from surface sediments of four Greenland lakes that further support this observation. Additionally, parallel downcore measurements of bulk carbonate and chironomid head capsule $\delta^{18}O$ values yielded very similar reconstructions of lake water isotopes through the late glacial at Rotsee (Switzerland) (Verbruggen et al., 2010). Given the fidelity of chironomid oxygen isotopes as a proxy for lake water, and the relationship between oxygen isotopes of precipitation and air temperature, we employ our down core record of oxygen isotopes measured from chironomids in Secret Lake to constrain the amplitude and timing of Holocene temperature trends and HTM warmth in northwest Greenland. This record also provides estimates of shifts in the stable isotopes of precipitation over northwest Greenland through the Holocene, providing an independent comparison with $\delta^{18}O$ records from nearby ice cores obtained from northern Greenland and the eastern Canadian Arctic.

2. Methods, study sites and materials

2.1. Study sites and field work

Modern lake water and surface (top 1 cm) sediment samples containing aquatic organic material from four Greenland lakes were collected in the summers of 2014 and 2015. Two lakes are in northwest Greenland, near Thule, and two are in southwest Greenland, near Nuuk (Table 1). Results from these new lakes add to existing datasets describing modern chironomid $\delta^{18}O$ – lake water relationships (Mayr et al., 2015; Verbruggen et al., 2011). Surface sediments were recovered using a 6″ x 6” Ekman dredge. Water samples from lakes, their inflows and, when available, precipitation were collected at surface sediment sites. Lake water and inflow samples were collected in 10 mL zero headspace glass vials or 30 mL HDPE Nalgene bottles, and taped to prevent evaporation. Samples from lakes and inflows were collected by hand up to 30 cm below the water surface. Snow from a single storm in 2014 was gathered from the ground (<12 h after snowfall in late August) into a 1000 mL Nalgene bottle and taped.

Secret Lake (informal name; 76.5798°N, 68.6619°W, Fig. 1) is a shallow (3.4 m maximum depth) 0.05 km^2 lake, situated 250 m above sea level and above the local marine limit. The lake is < 2 km from Wolstenholme Fjord and ~50 km from the open waters of Baffin Bay. Secret Lake is currently precipitation fed by a 0.5 km^2 watershed. This catchment includes several small (1 m^2) connected pools along the main inflow NE of the lake, all of which are precipitation fed as well. The active layer of Thule's continuous permafrost is between 0 and 2 m (Bjella, 2013). Additionally, Secret Lake's small catchment is elevated well above local river systems (Fig. 1), precluding inputs from any other source, including outlet glaciers of the GrIS. Since regional deglaciation around 10.7 ka, there is no evidence that the ice sheet, now 13 km away, advanced far enough to enter the present day watershed (Corbett et al., 2015, 2016). The lake is ice-covered for much of the year but overflows into a surface outflow stream during the ice-free summer months, including during our visits to the site in late August of both 2014 and 2015. All of these aforementioned catchment characteristics make Secret Lake an excellent candidate to reconstruct past isotopes of precipitation.

We recovered a 1.44 m sediment core (core 14-SEC-N1) from 3.36 m water depth in Secret Lake using a hammer driven Nesje piston system in August 2014. Coring stopped when we met resistance and repeated hammering did not advance the core tube further into the sediment. We bagged the top 2–3 cm of sediment, including the sediment water interface while recovering the core in the field. Basal sediments are dense diatomaceous clay with abundant aquatic moss material. We also acquired an accompanying surface sediment sample (top 0–1 cm) using an Ekman dredge less than 2 m from the core site.

Despite the shallow depth of the lake, and wind storms in excess of 70 knots that occurred less than 1 week prior to sampling, wave action does not appear to have disturbed surface sediments, as laminated stratigraphy is intact in the top 5 cm of a nearby surface core. Water column clarity measured shortly after the storm using a Secchi disk was ~3 m, further evidence that widespread suspension of sediments by wave action is not problematic even in this relatively shallow lake.

Secret Lake is less than 6 km distance and less than 100 m different in elevation from Thule Air Base (TAB), where long term historical climate monitoring provides valuable information for interpreting our modern and paleo $\delta^{18}O$ record. Daily temperatures, relative humidity and precipitation are available from the TAB meteorological station from 1951 to 2012. Mean annual air temperatures (MAAT), mean July temperatures (MJT) and mean annual precipitation (MAP) at TAB are −11 ± 1.3 °C, 6 ± 1.2 °C and 184 ± 56 mm mean water equivalent per year (mm w.e. yr^{-1}) respectively. Additionally, an International Atomic Energy Agency (IAEA) monitoring station at TAB collected monthly temperature and $\delta^{18}O/\delta D$ values of precipitation from 1966 to 1971, accessible through the IAEA's Global Network of Isotopes in Precipitation online portal (IAEA/WMO, 2015).

2.2. Geochronology

The 14-SEC-N1 chronology is based upon six AMS ^{14}C ages on cleaned, hand-picked aquatic moss remains. Ages were calibrated using Calib 7.1 and IntCal13 (Reimer et al., 2013; Stuvier et al., 2005). The age-depth model was developed with the Bacon package in R, which uses Bayesian statistics to calculate probable sedimentation rates (Blaauw and Christen, 2011). The final age depth model output is produced using over 7 million iterations (Fig. 2).

2.3. Preparation of chironomids for $\delta^{18}O$ measurements

Two to 4 g aliquots of bulk sediment, representing 0.5–1.5 cm of

Table 1
Greenland lakes where surface sediments and lake-water were sampled in August 2014 or 2015.

Lake Name	Latitude (°N)	Longitude (°W)	Depth (m)	Surface Elevation (m a.s.l.)	$\delta^{18}O_{lake\ water}$	$\delta D_{lake\ water}$	$\delta^{18}O_{\ chironomids\ (0–1\ cm)}$
Secret Lake	76.58021	−68.65907	3.2	250	−18.5	−143.3	3.8
Stardam	76.66512	−67.94100	5.25	221	−19.2	−151.1	2.9
T1	63.757	−51.356	9	25	−15.2	−104.5	10.5
T2	63.757	−51.364	11	43	−15.3	−104.7	9.3

T1 and T2 are informal names. All lakes are isolated from glacial meltwater. $\delta^{18}O/\delta D$ values are reported in per mil, relative to VSMOW.

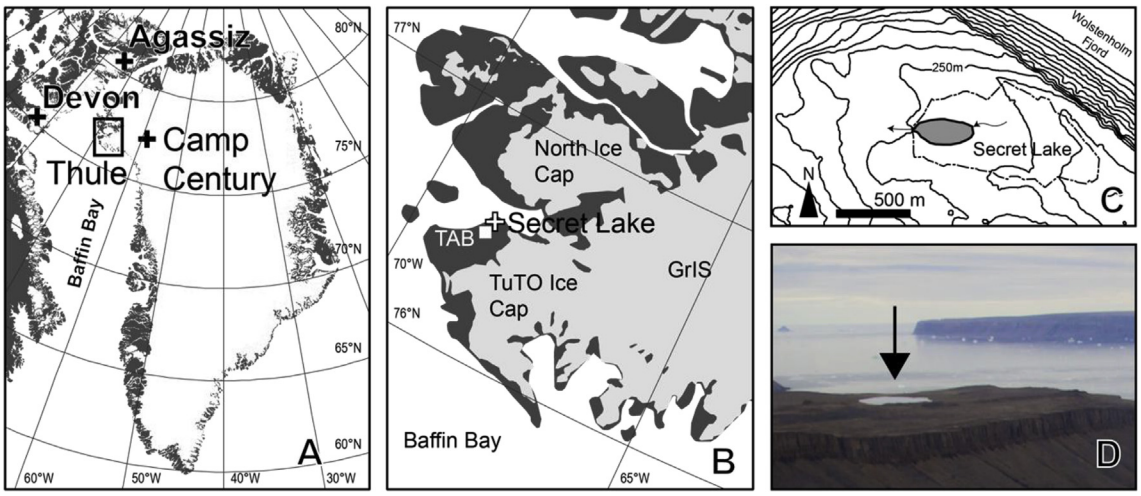

Fig. 1. A: Location of Thule, Greenland and the Agassiz, Devon and Camp Century ice core sites. B: Regional map of the Thule region with major glacial features and Secret Lake. GrIS is the Greenland Ice Sheet, TAB is Thule Air Base. Shaded light grey areas represent modern glaciers/ice sheets, and dark grey represents ice-free land. C: Local topography around Secret Lake. Contours are at 20 m intervals (asl). The dashed line represents Secret Lake's watershed. D: Oblique aerial view of Secret Lake indicated by the arrow looking west towards Baffin Bay in the distance.

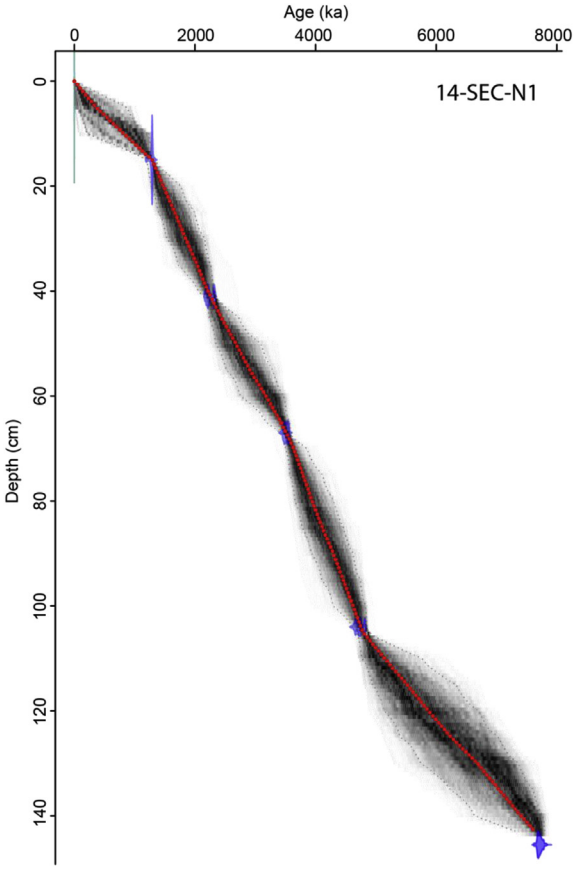

Fig. 2. Age-depth model for 14-SEC-N1, with calibrated ^{14}C dates and their respective probability density functions (transparent blue) and inferred modern surface (green bar). Darker greys indicate more likely calendar ages bounded by 95% confidence intervals; the red curve shows the single 'best' model based on the weighted mean age for each depth. (For interpretation of the references to colour in this figure legend, the reader is referred to the web version of this article.)

core depth, were deflocculated in a 10% KOH solution at 20 °C for 30 min. Processed sediment was thoroughly rinsed with DI water over a 150 μm sieve, and then chironomid remains were independently hand-picked, checked and cleaned of any remaining adhering sedimentary material. Wet remains were transferred to Nanopure water in pre-weighed and oven dried 3.2 × 4 mm lightweight Elemental Microanalysis® silver capsules. Filled capsules were crimped gently, freeze dried for at least 5 days immediately prior to isotope measurements, and then reweighed to determine the dry sample mass. We picked 150 to 200 individual head capsules for each sample to obtain adequate mass (between 150 and 200 μg) for these analyses.

Hot acid and alkali baths (60–70 °C) proposed by Wang et al. (2009) have been shown to both preferentially remove the chitin and protein moieties from modern whole insects (including head capsules) during pre-treatment, and potentially induce oxygen exchange with laboratory water. This may result in erroneous oxygen isotope values depending on whether chitin or protein was removed during processing, or whether lab water oxygen was exchanged with cuticles (Verbruggen et al., 2009). In contrast, cool (20 °C) alkali baths were shown by Verbruggen et al. (2009) to not significantly affect the $\delta^{18}O$ values of head capsules.

To assess whether pretreatment to remove carbonate was needed for our samples, we analyzed subfossil head capsules at 7 levels (0, 10, 35, 55, 96, 118 and 143 cm) throughout the core to check for the presence of adhering carbonates using Fourier Transform Infrared Spectroscopy (FT-IR). Head capsules were cleaned with KOH and DI water as described above, then 3 to 4 whole subfossils from each depth subsample were individually scanned using a Bruker Hyperion 2000 series FT-IR Microscope system between 600 and 4000 cm^{-1} at 32 times per 4 cm^{-1} resolution. Peaks at ~712, ~862 and ~1440 cm^{-1} are characteristic of carbonate and correspond to the in-plane bending vibration, the out-of-plane bending vibration and the asymmetric stretching of bonds in a CO_3^{2-} molecule, respectively (Liu et al., 2013; Reig et al., 2002; Xia et al., 2015). These characteristic carbonate peaks were not present in the spectra of any samples (representative spectrum are shown in Fig. 3). Geologic surveys of the area also indicate no carbonate bedrock in our study area (Dawes, 2006). Considering the results of visual and FT-IR inspection of head capsules, and the possible effects of acid pretreatment on chironomid exoskeletons, as suggested by Verbruggen et al. (2009), we did not treat chironomids with HCl.

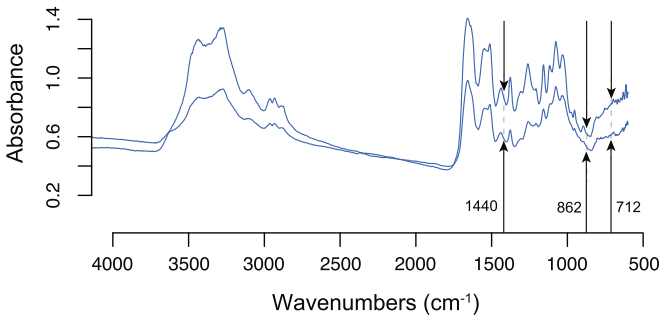

Fig. 3. Fourier Transform Infrared Spectroscopy (FT-IR) spectrum characteristic of chironomid head capsules from the 14-SEC-N1 core. The absence of peaks at ~712, 862 and 1440 cm^{-1} indicate that carbonates are not adhering to head capsules prior to oxygen isotope analysis.

2.4. Preparation of aquatic moss for $\delta^{18}O$ measurements

Past studies exploring the relationship between aquatic plants and host waters have typically isolated the cellulose component from aquatic plant remains for $\delta^{18}O$ analysis (Deniro and Epstein, 1981; Mayr et al., 2015; Sauer et al., 2001). Such extraction methods address the uncertainties that arise from different isotope effects in the various compounds that make up bulk plant material. Nonetheless, recent investigations into $\delta^{18}O$ values of bulk aquatic moss remains show strong correlations with isolated cellulose from the same sample, within ~1‰ (Jones et al., 2014; Zhu et al., 2014). Subfossil mosses (*Warnstorfia exannulata*) were picked from the Secret Lake core and thoroughly cleaned with DI water, then soaked in a 10% HCl solution at room temperature for 1 h. We did not treat the samples with HF as described in Zhu et al. (2014) due to the demonstrated lack of carbonates in the watershed, but all samples were rinsed again with DI water, then inspected for any remaining adhering material under a 30 × dissecting microscope. Leaves were then removed manually, isolating 70–120 μg of stem for isotope analysis. Typically, a single stem section was used, however, in the upper 20 cm of the core, multiple stem remains were often required to achieve sufficient mass. Samples were then placed in water in silver capsules and freeze-dried as described for chironomid head capsules above.

2.5. $\delta^{18}O$ analysis

The oxygen isotope composition of chironomid head capsules and moss stems were measured using a Thermo Scientific™ High Temperature Conversion Elemental Analyzer (TC-EA) coupled to a Thermo Scientific™ Delta V Isotope Ratio Mass Spectrometer (IRMS). Standards of known oxygen isotopic composition (IAEA-CH3, IAEA-CH6, IU Benzoic acid, NBS-127 and IAEA-SO5) were analyzed among all unknown sample runs. Additionally, we analyzed a previously unknown internal chitin standard, acquired from Sigma-Aldrich, due to its stoichiometric similarity to our unknown chironomid head capsules. Duplicate analyses of standards yielded analytical errors of 0.33‰ for the IRMS run in which we analyzed chironomid remains, and 0.41‰ for the run analyzing moss remains. Duplicate analyses of unknown materials down core yielded sample to sample errors of 0.52‰ for chironomids and 0.4‰ for the mosses. All $\delta^{18}O$ values are reported as per mil (‰) relative to VSMOW.

Modern lake water and precipitation isotopes were analyzed with a Picarro L2130-*i* Analyzer. Field samples (taped 10 mL bottles with zero headspace) were transferred to septum-capped vials, injected into a heated vaporizer, and then analyzed via cavity ring-down spectroscopy (Gupta et al., 2009). Repeated (8×) 1.2 μL injections for standards across all runs yielded analytical uncertainties < 0.08‰, and unknown sample to sample errors of 0.17‰.

3. Results

3.1. Core description and geochronology

Core 14-SEC-N1 is composed of 144 cm of banded (1–3 cm bands) grey to light brown gyttja. Coarse plant remains are preserved throughout the core, but decrease in abundance towards the top 20 cm, which is also characterized by finer, darker laminae (<0.5 cm). Plant material down core is dominantly aquatic moss stems. These subfossil plant remains as well as modern mosses acquired during the 2014 field season are *Warnstorfia exannulata*, common in high latitude Arctic lakes, often forming extensive mats across lake bottoms (Ole Bennike, pers comm; Guo et al., 2013).The six AMS ^{14}C results provide a millennial scale age-depth model and sedimentation history. No ages were considered outliers, and replicate basal moss samples yielded identical calibrated ages of 7730 yr (Table 2). The mean sedimentation rate for Secret Lake is 50 yrs cm^{-1}. From 7.7 ka to 5 ka, rates are slightly lower at 75 yrs cm^{-1}. From 5 ka to about 1.8 ka, rates increase to between 30 and 40 yrs cm^{-1}. Rates once again decrease to 90 yrs cm^{-1} from 1.8 ka to the top of the core.

3.2. $\delta^{18}O$ values of Thule-region precipitation and lake water

The relationship between average annual $\delta^{18}O$ of precipitation and mean annual surface temperature calculated from several years of historical (1966–1971) IAEA GNIP monitoring at TAB is 0.44‰ $°C^{-1}$ ($r^2 = 0.66$) (Fig. 4; IAEA/WMO, 2015). Continuous meteorological monitoring at TAB from 1952 through 2012 indicates that 29 and 35% of annual precipitation in the Thule area falls during the summer and autumn months, respectively (Wong et al., 2015). When monthly precipitation amounts (and their corresponding isotope values) are weighted with respect to total annual precipitation, the slope is marginally steeper at 0.46‰ $°C^{-1}$ ($r^2 = 0.69$), reflecting the greater influence of summer and autumn precipitation. These local relationships from time series are more shallow than the global spatial relationship (0.67‰ $°C^{-1}$) documented by Dansgaard (1964). Previously estimated Greenland isotope-temperature relationships for precipitation over the last 9000 years, however, appear to be more comparable to what we observe for Thule GNIP samples than to the global spatial relationship. Studies comparing Greenland ice core $\delta^{18}O$ values with borehole temperature inversions from Greenland ice cores during the Holocene, and gas occlusion based methods before the last glacial termination converge on a relationship between 0.44 and 0.53‰ $°C^{-1}$ (Buizert et al., 2014; Dahl-Jensen, 1998; Vinther et al., 2009). Seasonal relationships between temperature and $\delta^{18}O$ values of precipitation from the Thule IAEA data vary between 0.25‰ $°C^{-1}$ for autumn to 0.73‰ $°C^{-1}$ for winter (Table 3). Large seasonal changes in this relationship are expected in the high Arctic where the temperature and other climatic differences between winter and summer are more extreme than much of the world (Rozanski et al., 1993).

Modern lake water we collected in late summer from Thule-region lakes, including Secret Lake, is isotopically similar to both the mean historical (IAEA GNIP) summer precipitation and the 2014 summer precipitation sample that we collected from a single snowstorm. The measured $\delta^{18}O$ value of surface water from Secret Lake in August 2014 was −18.4‰, within 0.5‰ of mean historical summer (JJA) precipitation values (−18.9‰). Secret Lake surface

Table 2
Radiocarbon ages from Secret Lake.

Core	Depth (cm)	Lab Number	Material Dated	Fraction Modern	$\delta^{13}C$ (‰ PDB)	Radiocarbon Age (^{14}C yr BP)	Calibrated Age (cal yr BP)
14-SEC-N1	15.5–16	OS-115371	Plant Macrofossils	0.8437 ± 0.0019	−29.6	1360 ± 20	1290 ± 10
14-SEC-N1	41.5–42.5	OS-115372	Plant Macrofossils	0.7558 ± 0.0017	−29.8	2250 ± 20	2250 ± 80
14-SEC-N1	68–68.5	OS-115478	Plant Macrofossils	0.6649 ± 0.0016	−31.0	3280 ± 20	3510 ± 40
14-SEC-N1	104–105	OS-115479	Plant Macrofossils	0.5943 ± 0.0016	−28.9	4180 ± 20	4730 ± 90
14-SEC-N1	146–147	OS-115480	Plant Macrofossils	0.4249 ± 0.0015	−28.5	6880 ± 30	7730 ± 65
14-SEC-N1	146–147	OS-125562	Plant Macrofossils	0.4239 ± 0.0012	Not reported	6890 ± 25	7730 ± 60

Calibrated ages are reported as the midpoint of the 2σ range ± ½ of 2σ range.

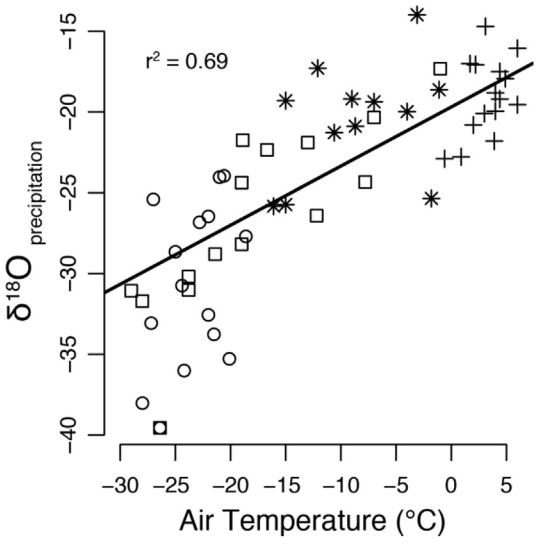

Fig. 4. Monthly (1966–1971) $\delta^{18}O$ values of precipitation and temperature measurements for Thule from WMO - IAEA/GNIP. Open circles are winter (DJF) measurements, open squares are spring (MAM), cross symbols are summer (JJA) and stars are autumn (SON). The solid black line is a linear regression fit representing the annual $\delta^{18}O$ values of precipitation – temperature relationship, weighted to the amount of precipitation (0.46‰ $°C^{-1}$).

water falls on the local meteoric water line as defined by available IAEA data (Fig. 5). The estimated lake volume is 93,000 m^3 fed by a 0.5 km^2 watershed. Annual precipitation of 184 ± 56 mm w.e. yr^{-1} from TAB meteorological records and compiled by Wong et al. (2015) suggest that (averaged since the start of the record in 1952) the Secret Lake watershed receives nearly 90,000 m^3 precipitation per year. Using these estimates, the mean residence time of lake waters in Secret Lake is approximately 1 year. Actual residence time presumably varies greatly throughout the year, with short effective residence time of cold-season precipitation during the rapid snowmelt period in spring (Woo, 1980).

3.3. $\delta^{18}O$ of modern chironomid remains

The $\delta^{18}O$ values of chironomid head capsules analyzed from surface sediments near Thule and Nuuk, paired with $\delta^{18}O$ values of modern lake water, have been added to a growing list of similar samples from around the world (Fig. 6). Combining our new data with the northern Europe (Verbruggen et al., 2011) and Patagonia data (Mayr et al., 2015), we calculate a biological fractionation factor (BFF) of 1.0224 – near identical to that calculated by Verbruggen et al. (2011) (1.0223) in 2011 but less than that estimated by early pilot studies (Wooller et al., 2004). Based on all available data including our new high Arctic sites, chironomids are 22.4 ± 1.3‰ higher relative to the lake water in which they grow. The strong correlation between lake water and head capsule $\delta^{18}O$ ($r^2 = 0.94$) is based on multiple studies thus far examining 38 lakes spanning 36° of Northern Hemisphere (NH) latitude (4° in the southern hemisphere) and a 27 °C range of mean annual surface temperature.

Given that chironomid head capsules consistently record lake water isotopic composition, and lake water (in appropriate settings) is influenced by the condensation temperature of watershed precipitation, oxygen isotopes measured in head capsules are a potential proxy for paleotemperature in lakes not greatly affected by evaporation (Wooller et al., 2004). Wooller et al. (2004) found that MAAT is highly correlated with the $\delta^{18}O$ values of chironomid head capsules in surface sediments of their four study lakes ($r^2 = 0.98$), with a slope of 0.65‰ $°C^{-1}$. The weaker relationship between $\delta^{18}O$ values of chironomids and MAAT found in all comparable data worldwide ($r^2 = 0.79$) likely reflects the differing, complex controls on oxygen isotopes of precipitation and ultimately lake water between sites (Fig. 7).

3.4. Analysis of downcore organic materials

$\delta^{18}O$ values of Secret Lake chironomids decreases by ~2‰ from the beginning of our record after 8 ka to the present, from an average of 5.5 to 3.8‰ (Fig. 8D). From 7.7 ka to around 4 ka, values are between 7 and 4.5‰ and then decrease gradually into the late Holocene. The lowest $\delta^{18}O$ values measured in the Secret Lake record occur between 1.2 ka and the present. The difference between the highest values and lowest values between 7.7 ka and 1.2 ka is just over 3‰. Downcore analysis of $\delta^{18}O$ values from *Warnstoria exannulata* stems yields a more variable record, but indicates a trend towards 2‰ lighter values after 4 ka (Fig. 8C). Although the $\delta^{18}O$ values of the *Warnstorfia exannulata* exhibits more sample-to-sample variability and a less coherent trend than chironomid $\delta^{18}O$, mean values after 4 ka are consistently lower. We can assume that

Table 3
Mean seasonal $\delta^{18}O$ values of Thule meteoric waters collected by the IAEA (1966–1971) and slopes of the $\delta^{18}O$-temperature relationships (WMO - IAEA/GNIP, 2015).

	Annual $\delta^{18}O$	Spring $\delta^{18}O$	Summer $\delta^{18}O$	Autumn $\delta^{18}O$	Winter $\delta^{18}O$
Average $\delta^{18}O$	−25.9	−25.9	−18.9	−21.1	−30.5
Max. $\delta^{18}O$	−14.0	−17.3	−14.7	−14.0	−24.0
Min. $\delta^{18}O$	−39.6	−39.6	−22.9	−25.8	−39.6
Seasonal T°C- ‰ Slope	0.44	0.57	0.59	0.25	0.73
Amount weighted T°C- ‰ Slope	0.46				

Spring is MAM, summer is JJA, autumn is SON, and winter DJF. $\delta^{18}O$ values are reported in per mil, relative to VSMOW.

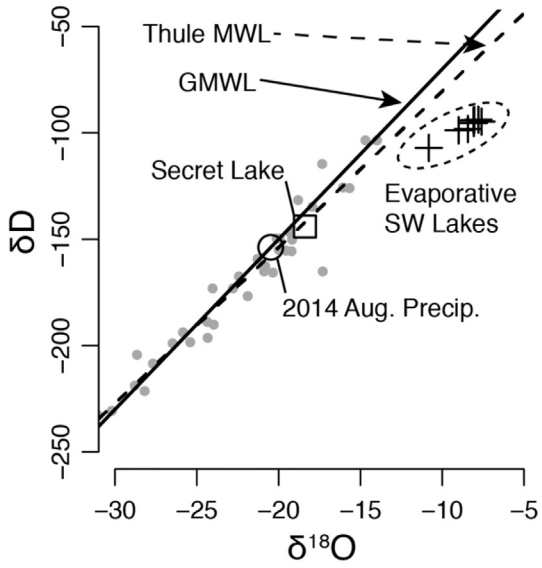

Fig. 5. Isotopes of Secret Lake (August 2014) lake water and August 2014 precipitation (a single snowstorm), compared with meteoric waters. Grey points are historical isotopes of precipitation from IAEA monitoring at Thule Air Base, 1966–1971; (WMO - IAEA/GNIP, 2015), GMWL is the global meteoric water line (Craig, 1961); The Thule MWL is a linear regression from the IAEA historical monitoring. Crosses are July 2014 lake water from SW Greenland lakes near Kangerlussuaq at the head of Sondre Stromfjord, where lakes are known to experience significant evaporative enrichment in a relatively warm, dry summer climate (Leng and Anderson, 2003). $\delta^{18}O/\delta D$ values are reported in per mil, relative to VSMOW.

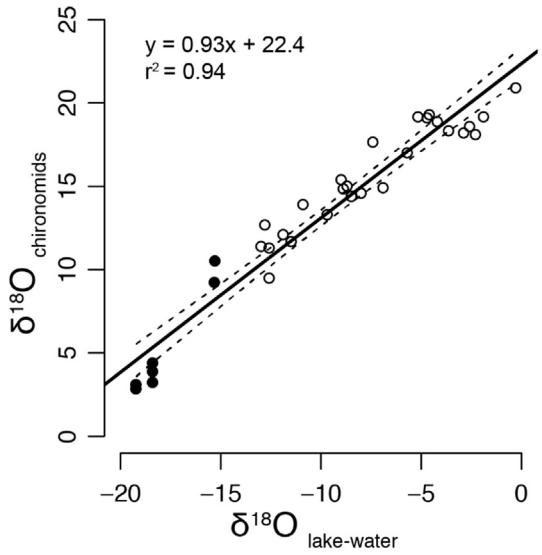

Fig. 6. Global relationship between $\delta^{18}O$ values of chironomid head capsules and lake waters with 95% confidence intervals. New data from Greenland surface sediments are plotted as solid circles. Previous field based studies by Verbruggen et al., 2011 and Mayr et al., 2015 are plotted as open circles. Wooller et al., 2004 do not report lake water $\delta^{18}O$ values. $\delta^{18}O$ values are reported in per mil, relative to VSMOW.

the aquatic mosses lack significant lignin (Sculthorpe, 1967) and are composed mainly of cellulose, and assume a cellulose - growth water fractionation of ~28‰ (Mayr et al., 2015; Sauer et al., 2001; Zhu et al., 2014). Thus our macrophyte data indicate a drop in average lake water $\delta^{18}O$ values from a maximum of −17 at the start of our record at 7.7 ka to −21‰ in the Neoglacial. As discussed above, chironomid head capsules are higher by 22.4‰ relative to growth water, so chironomids and mosses yield very similar

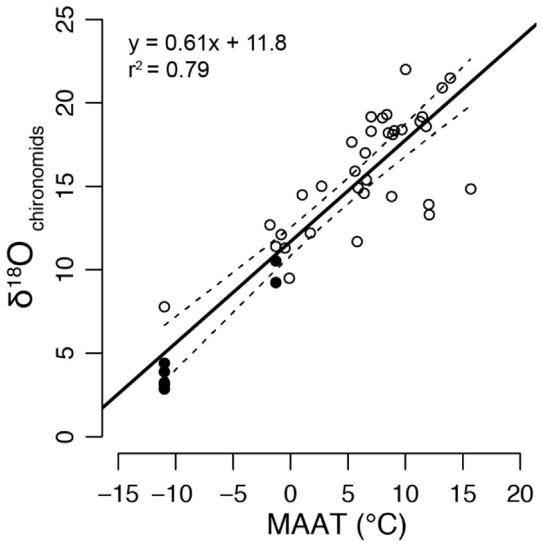

Fig. 7. Global relationship between $\delta^{18}O$ values of chironomids in surface sediments and mean annual air temperatures (MAAT) for each lake with 95% confidence intervals. New data from Greenland are plotted as solid circles. Previous field based studies by Wooller et al. (2004), Verbruggen et al. (2011) and Mayr et al. (2015) are plotted as open circles. $\delta^{18}O$ values are reported in per mil, relative to VSMOW.

reconstructed lake water composition throughout the Holocene. This lends confidence to reconstructions of both absolute lake water composition and the magnitude of the overall isotopic shift from early to late Holocene (Fig. 8F).

We place conservative constraints on temperature change based upon Secret Lake chironomid $\delta^{18}O$ by applying and comparing three $\delta^{18}O$ - temperature relationships: the global spatial relationship (Dansgaard, 1964), the Thule IAEA GNIP historical relationship (annual amount-weighted from 1966 to 1971), and the summer (JJA) relationship from the IAEA collections at Thule. These three estimates of the precipitation-temperature relationship (0.46–0.67‰ $°C^{-1}$) yield estimated temperature differences of 7 to 4.2 °C between the warmest and coldest parts of the past 7.7 ka. Relative to modern (i.e. the temperature inference from surface sediments), the isotopic data suggest that during the warmest period from 7.7 to 6 ka temperatures were 2.5–4 °C warmer than present, and during the last 1.2 kyr, the coldest period in our record, temperatures were 1.5–3 °C cooler than present (Fig. 9). As we describe in the Discussion below, these estimates are likely maximum constraints on the amplitude of temperature change experienced over these time periods.

4. Discussion

4.1. Modern observations of chironomid oxygen isotope composition

Data from this study combined with published research comparing lake water and modern chironomid $\delta^{18}O$ values around the world demonstrate the utility of oxygen isotopes measured in chironomid head capsules as a proxy for lake water oxygen isotopes. We find that $\delta^{18}O$ values of chironomid head capsules in Greenland lake surface sediments are higher relative to host waters by 22.4‰, consistent with enrichment factors elsewhere in the world. The 22.4‰ enrichment in head capsules from growth (lake) water shown by the aggregated global surface sediment dataset is consistent regardless of the many factors that can influence the isotopic composition of lake water, and the wide diversity of

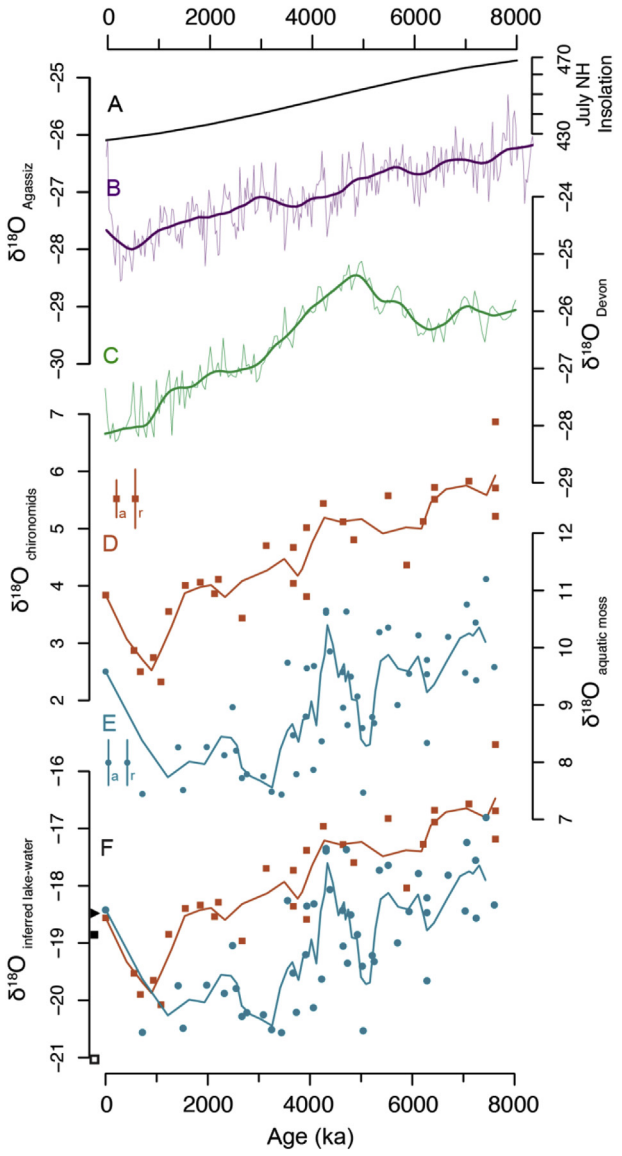

Fig. 8. Downcore results from Secret Lake and climate data from northwest Greenland. A: Northern Hemisphere July insolation in Wm^{-2}. B: Elevation corrected $\delta^{18}O$ from Agassiz Ice Cap (Lecavalier et al., 2017). C: $\delta^{18}O$ values from Devon Ice Cap (Koerner, 1977). D: $\delta^{18}O$ values of chironomid head capsules from Secret Lake with a 3 point moving average. The uppermost measurement at 0 yr is from a separate surface (0–1 cm) sample. E: $\delta^{18}O$ values of aquatic mosses from Secret Lake with a 3 point moving average. F: Inferred lake water from chironomid $\delta^{18}O$ (red points) and aquatic moss $\delta^{18}O$ values (blue points); shown on y-axis are measured August 2014 lake water (triangle) and mean historical summer and autumn precipitation (closed and open squares respectively (1966–1971; WMO - IAEA/GNIP, 2015). Analytical and replicate 1σ errors for measured materials in D and F are denoted 'a' and 'r' respectively. $\delta^{18}O$ values are reported in per mil, relative to VSMOW. (For interpretation of the references to colour in this figure legend, the reader is referred to the web version of this article.)

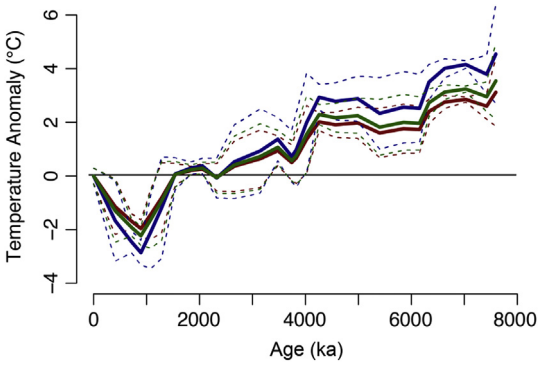

Fig. 9. Isotope-inferred temperature anomaly from Secret Lake using the local summer precipitation $\delta^{18}O$ – temperature relationship of 0.59‰ $°C^{-1}$ (green), the local annual amount weighted relationship of 0.46‰ $°C^{-1}$ (blue), and the global relationship of 0.67‰ $°C^{-1}$, (red). All estimates are bounded by ± 1σ. As discussed in the text, we view these estimates as upper bounds on the amplitude of past summer-biased temperature changes. (For interpretation of the references to colour in this figure legend, the reader is referred to the web version of this article.)

climate at the study sites, which span 27 °C MAAT and 20‰ in lake water $\delta^{18}O$ values. Unlike carbonate or diatoms (Leng and Henderson, 2013), chironomids may maintain a constant fractionation factor regardless of host water temperature (and presumably a correspondingly wide range of species assemblage composition), as demonstrated by our data and available literature.

As chironomid remains are widely preserved in lakes around the world, this proxy may prove valuable for reconstructing past lake water compositions in locations unsuitable for other isotope based methods, e.g. carbonate (Heiri et al., 2009, 2012). In addition to their widespread preservation, chironomid head capsules also have the advantage that they can be confidently isolated in a straightforward fashion, compared for example to diatoms (Leng and Henderson, 2013). As lacustrine species are obligate aquatic organisms, there is little concern about terrestrial contamination, compared for example to isolating cellulose. Chemically gentle sediment treatment protocols such as the method outlined above do not appear to alter the isotopic composition of the head capsule and are simpler than other methods, e.g. cellulose extractions. Care should be taken when working in watersheds containing carbonate bedrock, as precipitation of crystals may occur on the chironomid subfossils. For detailed discussion of treatment protocol experiments, see Verbruggen et al. (2009).

While recent data largely support fractionation effects independent of temperature, controlled laboratory culturing experiments could further enhance our understanding of any isotope effects during head capsule synthesis. Genus or species dependent effects have currently been quantified for carbon isotopes (van Hardenbroek et al., 2014), but it has not been fully explored whether this may be an issue with oxygen. In spite of these potential issues, there is great promise for this proxy to expand lake water isotope reconstructions to the many regions where chironomids are preserved, and in so doing, to allow for more widespread paleoclimate reconstructions.

4.2. *Interpreting chironomid and lake water $\delta^{18}O$ values at Secret Lake*

Given the hydrology and setting of Secret Lake, we have argued that its lake water isotopic composition primarily reflects the isotopic composition of precipitation, which in turn is strongly correlated with surface air temperature in northwest Greenland. We have also proposed that lake water at this site is summer and autumn biased, meaning that downcore trends dominantly reflect shifts in summer and autumn precipitation, with a lesser signal from winter and spring. This is in part because precipitation amount throughout the year (at least in the instrumental dataset) is weighted toward summer and autumn, with 64% of precipitation falling during the summer and autumn. Additionally, hydrologic inputs and outputs to the lake should essentially shut down during the long ice-covered period from mid-autumn through late spring. Upon thawing of ice cover, cold-season precipitation enters the lake mostly during the rapid spring melt (when residence time should

be shorter than the annual average) and summer precipitation likely lingers in the lake throughout the subsequent long, hydrologically inactive ice-covered season (Woo, 1980).

Lake water $\delta^{18}O$ samples collected in August 2014 have values indiscernible from mean historical (1966–1971) summer precipitation values for the Thule area (IAEA/WMO, 2015) (Tables 1 and 2, Fig. 5). Importantly, the relationship of the modern lake water to the meteoric water line (Fig. 5) suggests minimal enrichment from lake water evaporation in this through-flowing lake, even at the end of summer when evaporative influences likely peak just before lake ice cover resumes. Permafrost in the Thule area and in the vicinity of Secret Lake also limits groundwater flow within the small watershed, particularly from mid-autumn to early summer. In warmer south Greenland, freezing of the active layer by mid-September essentially halts any subsurface inputs to lakes (Leng and Anderson, 2003). These observations support the interpretation that lake water oxygen isotopes at this site primarily reflects contemporaneous precipitation isotopes. $\delta^{18}O$ values of lake water inferred from chironomid head capsules in Secret Lake surface sediments are comparable to both historical summer lake water $\delta^{18}O$ values (Fig. 8F), and from that of snow collected in late August 2014. Combined, these observations indicate that $\delta^{18}O$ values of chironomid head capsules at Secret Lake are best interpreted as a summer and early autumn-biased proxy for oxygen isotopes of precipitation, provided the amount and seasonality of precipitation falling within the watershed and entering the lake has been relatively stable through the Holocene.

The 3‰ decline between early and late Holocene in $\delta^{18}O$ values of chironomids from Secret Lake is larger than observed in the ice core record from Agassiz ice cap, Ellesmere Island 400 km to the W-NW (Fig. 8B). Isotopic shifts in Secret Lake more closely resemble the ice core record from Devon ice cap, Devon Island (Fig. 8E) (Koerner, 1977). $\delta^{18}O$ values in Agassiz ice cap declines by ~2‰ from 7.7 ka to the Neoglacial, interpreted as a cooling of 4 °C (Lecavalier et al., 2017). The $\delta^{18}O$ record from the Devon ice cap (not corrected for isostatic uplift) shows a 2.2‰ shift towards lower values after 5 ka. Our reconstruction of oxygen isotopes of precipitation in northwest Greenland suggests a greater positive temperature anomaly during the HTM than in these other records. This further supports our assertion that the Secret Lake chironomid $\delta^{18}O$ record is largely recording the warmest part of the year, since declining summer insolation was the dominant change in forcing at these latitudes through the Holocene.

Inferred lake-water reconstructions from moss and chironomid data are largely in agreement for the entire record. As noted in section 3.4, the moss $\delta^{18}O$ values exhibit greater variability than chironomids between 8 and 4 ka, followed by more consistent $\delta^{18}O$ trends thereafter. Aquatic moss samples were measured on 3–5 mm sections of multiple stems for each sample. Aquatic moss growth is seasonal and can be rapid, growing between 2 and 12 cm in high Arctic lakes during a summer (Guo et al., 2013). Our sampling of such small stem sections potentially captures only a portion of the growth season, and much less than the 25–50 years likely represented from chironomid data points, which may explain the greater sample-to-sample variability exhibited in the moss $\delta^{18}O$ data. Divergence between the moss and chironomid data could be due to enhanced summer cooling or increased winter temperatures (i.e. decreasing seasonality) through the Holocene.

Factors other than insolation-driven local surface temperature also play a role in determining precipitation and lake water isotopic composition over time. For example, marine sediment cores recovered in northern Baffin Bay indicate that sea ice cover and duration were reduced during the HTM (Ledu et al., 2008; Levac et al., 2001). Ice-free conditions from ~7 to 3.6 ka persisted for 4–5 months per year, compared with 1–2 months from 3.6 to the pre-industrial era (Levac et al., 2001). Less sea ice cover during the warmer earlier Holocene could conceivably have multiple effects. Higher regional temperatures from sea ice feedbacks over Baffin Bay, combined with an enhanced local precipitation source, could result in higher mean annual precipitation $\delta^{18}O$ values. Conversely, it has also been argued that reduced sea ice cover can enhance winter snowfall, delivering isotopically lower precipitation as an annual average (Thomas et al., 2016). Shifting dominant storm tracks through the Holocene could also play a role. The historical IAEA monitoring data from TAB reveal a pronounced decrease in $\delta^{18}O$ values of precipitation during March every year, and Osterberg et al. (2015) have documented that major shifts in regional storm tracks occur at that same time of year. This effect is also evident in other high Arctic sites such as Barrow, Alaska (Rozanski et al., 1993).

Changes in evaporative enrichment of lake water in a changing climate would also overprint the primary precipitation signal. For example, if warmer summers during the HTM caused more evaporation of lake water, that would cause an enhanced positive anomaly in lake water isotopic composition despite evidence that evaporation has a minimal effect on modern lake water. We suggest that the isotopic changes recorded through the Holocene at Secret Lake most likely place upper bounds on the amplitude of temperature changes over that period. This would be the case if warmer summers in the study area were accompanied by greater evaporative enrichment of lake water, as has been inferred elsewhere in Greenland for the early to middle Holocene (e.g. Anderson and Leng, 2004; Balascio et al., 2013), and/or characterized by a more proximal moisture source related to decreased sea ice.

$\delta^{18}O$ values of chironomid head capsules suggest upper bounds of HTM temperatures (represented as anomalies relative to modern from a 3 point moving average of the data) up to 2.5–4 °C warmer until ~6 ka (Fig. 9). A marked change in the climate regime around 4 ka is recorded by drops in $\delta^{18}O$ values of both chironomids and aquatic moss stems, although the latter yields a much more variable record overall.

Our upper estimates of the HTM temperature anomaly, in excess of 3 °C warmer than present, are inferred using the (1966–1971) local annual amount weighted $\delta^{18}O$ – temperature gradient for TAB of 0.46‰ $°C^{-1}$. This slope is within the range of reported Holocene relationships estimated across Greenland from ice cores (Buizert et al., 2014; Dahl-Jensen, 1998; Vinther et al., 2009). However, as discussed above, Secret Lake and other lakes in the region appear biased towards summer and autumn $\delta^{18}O$ of precipitation values. The summer season $\delta^{18}O$ – temperature slope in Thule is 0.59‰ $°C^{-1}$, and the global spatial slope is 0.67‰ $°C^{-1}$. Given uncertainty regarding what slope is most applicable to a Holocene reconstruction, we place conservative constraints on paleotemperatures by applying all three slopes to generate our temperature reconstruction (Fig. 9). We conclude that HTM warm-season temperatures were between 2.5 and 4 °C warmer than present from 7.7 (the beginning of the record) to 6 ka. Summer temperatures decreased further ~4 ka and then throughout the late Holocene, with the coldest inferred temperatures occurring after 1.2 ka.

4.3. Regional Holocene climate history

We find summer temperatures as much as 2.5–4 °C warmer than present during the HTM, based upon $\delta^{18}O$ values of aquatic chironomid larvae remains in a northwest Greenland lake. As the sediment core we recovered from Secret Lake is younger than 8 kyr, this record does not capture the onset of Holocene warmth, and may not capture the warmest part of the Holocene. Continual cooling after 4 ka led to coldest temperatures after 1.2 ka, with temperature anomalies 2–3 °C below present. Below we compare this reconstruction with inferences from different archives and

proxies throughout the region.

The warmest summer temperatures inferred from our isotope record are comparable in timing to peak August sea surface temperatures (SST) estimated in northern Baffin Bay, where warmer than present conditions prior to 4 ka have been attributed to greater insolation and persistent incoming warm water via the West Greenland Current (Ledu et al., 2008; Levac et al., 2001). 50–100% of the Agassiz Ice cap is composed of melted ice layers during the early Holocene, declining to <10% around 4 to 5 ka (Fisher et al., 1995). Closer to our study site, peat deposits on an island offshore of northwest Greenland suggest warmer-than-present summers from the early Holocene through ~5.1 ka (Bennike et al., 2008). Warm indicator beetle and fish remains in northwest Greenland record a warmer early Holocene from 8.8 to 7.5 ka, overlapping briefly with the Secret Lake record (Fredskild, 1985). The geographically closest quantitative temperature reconstruction is inferred from aggregated pollen records across north Greenland and indicates warmest July temperatures (~1 °C warmer than present) between 7 and 5 ka (Gajewski, 2015). We must look farther afield for additional quantification of HTM warmth: Approximately 1000 km to the south, a 2–3 °C July temperature anomaly (relative to present) between 6 and 5 ka was reported based upon chironomid assemblages near Illulisat and Jakobshavn (Axford et al., 2013). Across Baffin Bay on northeastern Baffin Island, HTM summer temperatures were an estimated ~5 °C warmer than the pre-industrial late Holocene and 3.5 °C warmer than present, based upon chironomid assemblages (Axford et al., 2009; Thomas et al., 2007). Both of the chironomid-based estimates are within (on the low end to middle of) the range of HTM temperature anomalies we reconstruct based upon oxygen isotopes.

Cold spells, the development of more extensive sea ice cover in Baffin Bay (Levac et al., 2001), and a decrease in sedimentation at Kap Inglefield Sø (250 km N of Thule) (Blake et al., 1992) after 4 ka are coincident with the gradual cooling recorded in the Secret Lake isotope record and presumably driven by summer insolation trends. Multiple high latitude climate records from Greenland and Arctic Canada synthesized by Briner et al. (2016) show a general regional shift to cooler conditions after 4 ka. A 3500-yr late Holocene record from Greenland's northernmost lake indicates coldest conditions there from 2.4 ka until the last century, in agreement with the timing of coldest conditions at Secret Lake (Perren et al., 2012). A cooling trend over the last two millennia of the pre-industrial Holocene has been widely documented across the Arctic (e.g. Kaufman et al., 2009).

Glacial geological evidence in the form of subfossil plants found in a nearby North Ice Cap shear plane dating to 5.53 ka suggest that the ice cap (40 km north from Secret Lake) was less extensive than present prior to that time (Goldthwait, 1960), with subsequent Neoglacial re-advance. Low LGM $\delta^{18}O$ values indicative of Pleistocene conditions have not been found along the eastern North Ice Cap and the western Tuto Ice Cap margins (Fig. 1), also supporting regional early Holocene ice retreat behind present-day margins (Reeh et al., 1990). Summer temperatures >2.5 °C warmer than present would presumably have driven significant retreat of these ice masses. Additional and more detailed glacial geologic investigations around the margins of North Ice Cap and the GrIS are currently underway (Kelly et al., 2015).

Improved constraints on the timing and magnitude of HTM warmth around Greenland can provide better input and tests for ice sheet sensitivity models. The HTM is a useful, albeit imperfect, recent analog for potential 21st Century warming. Following deglaciation, the GrIS retreated behind its present margins (by as much as 20–60 km in some parts of Greenland) during the HTM (Larsen et al., 2015; Young and Briner, 2015). Recent model experiments have imposed a hypothetical HTM temperature anomaly, in recognition that the isotope records from central Greenland ice cores did not yield reliable estimates of peak Holocene warmth (Lecavalier et al., 2014; Simpson et al., 2009). HTM temperatures inferred from ice core records were scaled up by 1–2 °C between 9 and 5 ka to maximize the fit between model results and observations of glacial advance and retreat across Greenland. However, the response of the ice sheet in the proximity of Camp Century (~200 km from Thule) is still not well represented with temperature parameterizations (Lecavalier et al., 2014, 2017). Warmer summers in the early Holocene than those imposed, such as the middle to upper end of the 2.5–4 °C summer temperature anomaly suggested by our dataset from northwest Greenland, could help account for the differences between the model and observed relative sea level change in the northwest. The recently revised $\delta^{18}O$ inferred temperature record from the Agassiz Ice Cap is in agreement with our temperature anomalies between 7.7 and 4 ka, with even warmer temperatures prior to 7.7 ka (Lecavalier et al., 2017). Our results may provide further insights on the elevation history at Camp Century and the resulting ice core $\delta^{18}O$ record.

5. Conclusions

This study builds upon previous methodological work by further demonstrating the utility of chironomid $\delta^{18}O$ values as a proxy for lake water $\delta^{18}O$ values and past climate change. $\delta^{18}O$ values of chironomid remains in surface sediments are higher by a consistent amount relative to modern lake waters across Europe, South America and, as we demonstrate, a range of latitudes in Greenland. The widespread preservation of chironomid remains in lakes worldwide can help expand reconstruction of lake water isotopes beyond sites where carbonate materials are preserved.

Oxygen isotopes measured in the subfossil remains of both chironomids and aquatic plants from a 7.7 kyr sediment record recovered from Secret Lake record a 3‰ decline in lake water $\delta^{18}O$ values between the early and late Holocene, with most of the decline occurring after ~4 ka. We argue that this isotopic shift provides a summer- and early autumn-biased maximum estimate of Holocene temperature changes over northwest Greenland. Inferred warm-season temperatures were 2.5–4 °C warmer than present from at least 7.7 ka to 4 ka, and the coldest part of the Holocene, after 1.2 ka, was 1.5–3 °C colder than present. The ranges of these estimates reflect uncertainty in the isotope-temperature relationship for precipitation through the Holocene. Due to the possible overprinting effects of enhanced evaporation and reduced sea ice in Baffin Bay (and thus a closer moisture source) during the HTM, the estimated anomaly of 2.5–4 °C between 7.7 and 4 ka is likely an upper limit, which (along with its summer bias) may explain why this estimate is slightly higher than from some other proxy records from the northern Baffin Bay region. The timing of temperature shifts at this study site in northwest Greenland appears consistent with published marine and terrestrial records from the surrounding region.

Peak Holocene warmth inferred from Secret Lake is also coincident with the documented retreat of regional glaciers, followed by readvance in the late Holocene. Additional ongoing paleoclimate and glacial investigations along the margin of the GrIS and local ice caps in northwest Greenland will further advance our understanding of ice sheet sensitivity to warming, and thus help to improve model capabilities in predicting future contributions of the GrIS to sea level rise.

Acknowledgements

Funding for this research was provided by National Science Foundation Grants PLR-1108303 and 1107411, a National

Geographic Explorers Grant 969415, a Geological Society of America Graduate Research Grant, the American Association of Geographers Marcus Fund, and the Institute for Sustainability and Energy at Northwestern. We thank A. Masterson, M. Osburn and K. Dutta for assistance with stable isotope analysis, G. Schellinger-Harrington and P. Kotecki for assistance with isolating chironomids for isotope analysis, O. Bennike for assistance identifying plant remains, N. Blair for assistance with FT-IR analysis, staff at LACCORE for core processing and WHOI-NOSAMS for radiocarbon analysis and two anonymous reviewers for helpful comments that improved the manuscript. Water isotopes were measured in M. Osburn's lab at Northwestern University. Field logistics were coordinated by Polar Field Services, particularly K. Cosper and J. Hurley. G. Bromley, L. Farnsworth, M. Jackson and A. Taylor assisted with field work. We thank the people and Government of Greenland (export permit 028/2014) and Thule Air Base for site access, and Air Greenland and the U.S. Air Force for transportation support.

References

Anderson, N.J., Leng, M.J., 2004. Increased aridity during the early Holocene in West Greenland inferred from stable isotopes in laminated-lake sediments. Quat. Sci. Rev. 23, 841–849.
Axford, Y., Briner, J.P., Miller, G.H., Francis, D.R., 2009. Paleoecological evidence for abrupt cold reversals during peak Holocene warmth on Baffin Island, Arctic Canada. Quat. Res. 71, 142–149.
Axford, Y., Losee, S., Briner, J.P., Francis, D.R., Langdon, P.G., Walker, I.R., 2013. Holocene temperature history at the western Greenland Ice Sheet margin reconstructed from lake sediments. Quat. Sci. Rev. 59, 87–100.
Balascio, N.L., D'Andrea, W.J., Bradley, R.S., Perren, B.B., 2013. Biogeochemical evidence for hydrologic changes during the Holocene in a lake sediment record from southeast Greenland. Holocene 23, 1428–1439.
Bennike, O., Goodsite, M., Heinemeier, J., 2008. Palaeoecology of Holocene peat deposits from Nordvestø, north-west Greenland. J. Paleolimnol. 40, 557–565.
Bjella, K., 2013. An investigation into a white painted airfield on permafrost: Thule air Base, Greenland, ISCORD 2013: planning for sustainable cold regions. ASCE 565–575.
Blaauw, M., Christen, A.J., 2011. Bacon.R, 2.2 Ed.
Blake, W., Boucherle, M., Fredskild, B., Janssens, J., Smol, J.P., 1992. The geomorphological setting, glacial history and Holocene development of "Kap Inglefield Sø", Inglefield land, north-west Greenland. Meddeles. Om. Gronl. 27.
Briner, J.P., McKay, N.P., Axford, Y., Bennike, O., Bradley, R.S., de Vernal, A., Fisher, D., Francus, P., Fréchette, B., Gajewski, K., Jennings, A., Kaufman, D.S., Miller, G., Rouston, C., Wagner, B., 2016. Holocene climate change in Arctic Canada and Greenland. Quat. Sci. Rev. 147, 340–364.
Buizert, C., Gkinis, V., Severinghaus, J.P., He, F., Lecavalier, B.S., Kindler, P., Leuenberger, M., Carlson, A.E., Vinther, B., Masson-Delmotte, V., White, J.W., Liu, Z., Otto-Bliesner, B., Brook, E.J., 2014. Greenland temperature response to climate forcing during the last deglaciation. Science 345, 1177–1180.
Corbett, L.B., Bierman, P.R., Lasher, G.E., Rood, D.H., 2015. Landscape chronology and glacial history in Thule, northwest Greenland. Quat. Sci. Rev. 109, 57–67.
Corbett, L.B., Bierman, P.R., Rood, D.H., 2016. Constraining multi-stage exposure-burial scenarios for boulders preserved beneath cold-based glacial ice in Thule, northwest Greenland. Earth Planet S. C. Lett. 440, 147–157.
Craig, H., 1961. Isotopic variations in meteoric waters. Science 133, 1702–1703.
Dahl-Jensen, D., 1998. Past temperatures directly from the Greenland ice sheet. Science 282, 268–271.
Dansgaard, W., 1964. Stable isotopes in precipitation. Tellus 16, 436–468.
Dawes, P., 2006. Geological Map of Greenland, 1: 500,000, Thule, Sheet 5, Geological Survey of Denmark and Greenland Map Series 2. Geological Survey of Denmark and Greenland, Danish Ministry of the Environment.
Deniro, M.J., Epstein, S., 1981. Isotopic composition of cellulose from aquatic organisms. Geochimica Cosmochimica Acta 45, 1885–1894.
Fisher, D.A., Koerner, R.M., Reeh, N., 1995. Holocene climatic records from Agassiz ice cap, Ellesmere island, Nwt, Canada. Holocene 5, 19–24.
Fredskild, B., 1985. The Holocene vegetational development of the tugtuligssuaq and qeqertat, northwest Greenland. Meddeles. Om. Gronl. Geosci. 14.
Gajewski, K., 2015. Quantitative reconstruction of Holocene temperatures across the Canadian arctic and Greenland. Glob. Planet. Change 128, 14–23.
Goldthwait, R., 1960. Study of Ice Cliff in Nunatarssuaq, Greenland, U.S. Army Snow, Ice and Permafrost Research Establishment Technical Report, vol. 39, p. 106.
Guo, C.-Q., Ochyra, R., Wu, P.-C., Seppelt, R.D., Yao, Y.-F., Bian, L.-G., Li, S.-P., Li, C.-S., 2013. Warnstorfia exannulata, an aquatic moss in the Arctic: seasonal growth responses. Clim. Change 119, 407–419.
Gupta, P., Noone, D., Galewsky, J., Sweeney, C., Vaughn, B.H., 2009. Demonstration of high-precision continuous measurements of water vapor isotopologues in laboratory and remote field deployments using wavelength-scanned cavity ring-down spectroscopy (WS-CRDS) technology. Rapid communications in mass spectrometry. RCM 23, 2534–2542.
Heiri, O., Schilder, J., Van Hardenbroek, M., 2012. Stable isotopic analysis of fossil chironomids as an approach to environmental reconstruction: state of development and future challenges. Fauna nor. 31.
Heiri, O., Wooller, M., van Hardenbroek, M., Wang, Y., 2009. Stable isotopes in chitinous fossils of aquatic invertebrates. Pages news 17, 100–102.
IAEA/WMO, 2015. Global Network of Isotopes in Precipitation. The GNIP Database. Accessible at. http://www.iaea.org/water.
Jones, M.C., Wooller, M., Peteet, D.M., 2014. A deglacial and Holocene record of climate variability in south-central Alaska from stable oxygen isotopes and plant macrofossils in peat. Quat. Sci. Rev. 87, 1–11.
Kaufman, D.S., Axford, Y.L., Henderson, A.C.G., McKay, N.P., Oswald, W.W., Saenger, C., Anderson, R.S., Bailey, H.L., Clegg, B., Gajewski, K., Hu, F.S., Jones, M.C., Massa, C., Routson, C.C., Werner, A., Wooller, M.J., Yu, Z., 2016. Holocene climate changes in eastern Beringia (NW North America) – a systematic review of multi-proxy evidence. Quat. Sci. Rev. 147, 312–339.
Kaufman, D.S., Schneider, D.P., McKay, N.P., Ammann, C.M., Bradley, R.S., Briffa, K.R., Miller, G.H., Otto-Bliesner, B.L., Overpeck, J.T., Vinther, B.M., 2009. Recent warming reverses long-term arctic cooling. Sci. (New York, N.Y.) 325, 1236–1239.
Kelly, M.A., Osterberg, E.C., Axford, Y., Farnsworth, L., Howley, J.A., Lasher, G.E., Zimmerman, S., 2015. Holocene fluctuations of North Ice Cap, a proxy for climate conditions along the northwestern margin of the Greenland Ice Sheet. In: AGU Fall Meeting (San Francisco, California).
Koerner, R.M., 1977. Devon Island ice cap: core stratigraphy and paleoclimate. Science 196, 15–18.
Larsen, N.K., Kjaer, K.H., Lecavalier, B., Bjork, A.A., Colding, S., Huybrechts, P., Jakobsen, K.E., Kjeldsen, K.K., Knudsen, K.L., Odgaard, B.V., Olsen, J., 2015. The response of the southern Greenland ice sheet to the Holocene thermal maximum. Geology 43, 291–294.
Lecavalier, B.S., Fisher, D.A., Milne, G.A., Vinther, B.M., Tarasov, L., Huybrechts, P., Lacelle, D., Main, B., Zheng, J., Bourgeois, J., Dyke, A.S., 2017. High Arctic Holocene temperature record from the Agassiz ice cap and Greenland ice sheet evolution. Proc. Natl. Acad. Sci. U. S. A. 114, 5952–5957.
Lecavalier, B.S., Milne, G.A., Simpson, M.J.R., Wake, L., Huybrechts, P., Tarasov, L., Kjeldsen, K.K., Funder, S., Long, A.J., Woodroffe, S., Dyke, A.S., Larsen, N.K., 2014. A model of Greenland ice sheet deglaciation constrained by observations of relative sea level and ice extent. Quat. Sci. Rev. 102, 54–84.
Lecavalier, B.S., Milne, G.A., Vinther, B.M., Fisher, D.A., Dyke, A.S., Simpson, M.J.R., 2013. Revised estimates of Greenland ice sheet thinning histories based on ice-core records. Quat. Sci. Rev. 63, 73–82.
Ledu, D., Rochon, A., de Vernal, A., St-Onge, G., 2008. Palynological evidence of Holocene climate change in the eastern Arctic: a possible shift in the Arctic oscillation at the millennial time scale. This article is one of a series of papers published in this Special Issue on the themePolar Climate Stability Network Can. J. Earth Sci. 45, 1363–1375.
Leng, M.J., Anderson, N.J., 2003. Isotopic variation in modern lake waters from western Greenland. Holocene 13, 605–611.
Leng, M.J., Henderson, A.C.G., 2013. Recent advances in isotopes as palaeolimnological proxies. J. Paleolimnol. 49, 481–496.
Levac, E., Vernal, A.D., Blake Jr., W., 2001. Sea-surface conditions in northernmost Baffin Bay during the Holocene: palynological evidence. J. Quat. Sci. 16, 353–363.
Liu, X., Colman, S.M., Brown, E.T., Minor, E.C., Li, H., 2013. Estimation of carbonate, total organic carbon, and biogenic silica content by FTIR and XRF techniques in lacustrine sediments. J. Paleolimnol. 50, 387–398.
Mayr, C., Laprida, C., Lücke, A., Martín, R.S., Massaferro, J., Ramón-Mercau, J., Wissel, H., 2015. Oxygen isotope ratios of chironomids, aquatic macrophytes and ostracods for lake-water isotopic reconstructions – results of a calibration study in Patagonia. J. Hydrology 529, 600–607.
Osterberg, E.C., Hawley, R.L., Wong, G., Kopec, B., Ferris, D., Howley, J., 2015. Coastal ice-core record of recent northwest Greenland temperature and sea-ice concentration. J. Glaciol. 61, 1137–1146.
Perren, B.B., Wolfe, A.P., Cooke, C.A., Kjaer, K.H., Mazzucchi, D., Steig, E.J., 2012. Twentieth-century warming revives the world's northernmost lake. Geology 40, 1003–1006.
Reeh, N., Thomsen, H., Frich, P., Clausen, H., 1990. Stable isotope studies on the ice margins in the Thule area. In: Funder, S.V. (Ed.), Meddelesler om Gronland, Geoscience, pp. 47–63.
Reig, F.B., Adelantado, J.V.G., Moreno, M.C.M.M., 2002. FTIR quantitative analysis of calcium carbonate (calcite) and silica (quartz) mixtures using the constant ratio method. Application to geological samples. Talanta 58, 811–821.
Reimer, P.J., Bard, E., Bayliss, A., Beck, J.W., Blackwell, P.G., Ramsey, C.B., Buck, C.E., Cheng, H., Edwards, R.L., Friedrich, M., 2013. IntCal13 and Marine13 radiocarbon age calibration curves 0–50,000 years cal BP. Radiocarbon 55, 1869–1887.
Rozanski, K., Araguás-Araguás, L., Gonfiantini, R., 1993. Isotopic patterns in modern global precipitation, 78, 1–36.
Sauer, P.E., Miller, G.H., Overpeck, J.T., 2001. Oxygen isotope ratios of organic matter in arctic lakes as a paleoclimate proxy: field and laboratory investigations. J. Paleolimnol. 25, 43–64.
Sculthorpe, C.D., 1967. The Biology of Aquatic Vascular Plants. Edward Arnold Publishers, London.
Simpson, M.J.R., Milne, G.A., Huybrechts, P., Long, A.J., 2009. Calibrating a glaciological model of the Greenland ice sheet from the Last Glacial Maximum to

present-day using field observations of relative sea level and ice extent. Quat. Sci. Rev. 28, 1631–1657.
Stuvier, M., Reimer, P.J., Reimer, R.W., 2005. CALIB 7.1. WWW program and documentation.
Stocker, T.F., Qin, D., Plattner, G.-K., Tignor, M., Allen, S.K., Boschung, J., Nauels, A., Xia, Y., Bex, V., Midgley, P.M., 2013. Climate Change 2013: The Physical Science Basis. Intergovernmental Panel on Climate Change, Working Group I Contribution to the IPCC Fifth Assessment Report (AR5). Cambridge Univ Press, New York.
Thomas, E.K., Axford, Y., Briner, J.P., 2007. Rapid 20th century environmental change on northeastern Baffin Island, Arctic Canada inferred from a multi-proxy lacustrine record. J. Paleolimnol. 40, 507–517.
Thomas, E.K., Briner, J.P., Ryan-Henry, J.J., Huang, Y., 2016. A major increase in winter snowfall during the middle Holocene on western Greenland caused by reduced sea ice in Baffin Bay and the Labrador Sea. Geophys. Res. Lett. 43, 5302–5308.
van Hardenbroek, M., Lotter, A.F., Bastviken, D., Andersen, T.J., Heiri, O., 2014. Taxon-specific δ13C analysis of chitinous invertebrate remains in sediments from Strandsjön, Sweden. J. Paleolimnol. 52, 95–105.
Verbruggen, F., Heiri, O., Reichart, G.-J., Lotter, a.F., 2010. Chironomid δ18O as a proxy for past lake water δ18O: a Lateglacial record from Rotsee (Switzerland). Quat. Sci. Rev. 29, 2271–2279.
Verbruggen, F., Heiri, O., Reichart, G.J., Blaga, C., Lotter, a.F., 2011. Stable oxygen isotopes in chironomid and cladoceran remains as indicators for lake water δ18O. Limnol. Oceanogr. 56, 2071–2079.
Verbruggen, F., Heiri, O., Reichart, G.J., Leeuw, J.W., Nierop, K.G.J., Lotter, A.F., 2009. Effects of chemical pretreatments on δ18O measurements, chemical composition, and morphology of chironomid head capsules. J. Paleolimnol. 43, 857–872.
Vinther, B.M., Buchardt, S.L., Clausen, H.B., Dahl-Jensen, D., Johnsen, S.J., Fisher, D.a., Koerner, R.M., Raynaud, D., Lipenkov, V., Andersen, K.K., Blunier, T., Rasmussen, S.O., Steffensen, J.P., Svensson, a.M., 2009. Holocene thinning of the Greenland ice sheet. Nature 461, 385–388.
Wang, Y.V., O'Brien, D.M., Jenson, J., Francis, D., Wooller, M.J., 2009. The influence of diet and water on the stable oxygen and hydrogen isotope composition of Chironomidae (Diptera) with paleoecological implications. Oecologia 160, 225–233.
Wong, G.J., Osterberg, E.C., Hawley, R.L., Courville, Z.R., Ferris, D.G., Howley, J.A., 2015. Coast-to-interior gradient in recent northwest Greenland precipitation trends (1952–2012). Environ. Res. Lett. 10, 114008.
Woo, M., 1980. Hydrology of a small Lake in the Canadian high arctic. Arct. Alp. Res. 227–235.
Wooller, M.J., Francis, D., Fogel, M.L., Miller, G.H., Walker, I.R., Wolfe, A.P., 2004. Quantitative paleotemperature estimates from d18O of chironomid head capsules preserved in arctic lake sediments. J. Paleolimnol. 267–274.
Xia, M.S., Yao, Z.T., Ge, L.Q., Chen, T., Li, H.Y., 2015. A potential bio-filler: the substitution effect of furfural modified clam shell for carbonate calcium in polypropylene. J. Compos. Mater. 49, 807–816.
Young, N.E., Briner, J.P., 2015. Holocene evolution of the western Greenland Ice Sheet: assessing geophysical ice-sheet models with geological reconstructions of ice-margin change. Quat. Sci. Rev. 114, 1–17.
Zhu, J., Lücke, A., Wissel, H., Mayr, C., Ohlendorf, C., Zolitschka, B., 2014. Characterizing oxygen isotope variability and host water relation of modern and subfossil aquatic mosses. Geochimica Cosmochimica Acta 130, 212–228.